

On Galaxies and Homology

Gregory S. Novak,^{1,2,3*} Patrik Jonsson,^{4,5} Joel R. Primack,⁵
Thomas J. Cox,⁶ and Avishai Dekel,⁷

¹*Observatoire de Paris, LERMA, CNRS, 61 Av de l'Observatoire, 75014, Paris, France*

²*Department of Astrophysical Sciences, Princeton University, Princeton NJ, 08544*

³*UCO/Lick Observatories, University of California, 1156 High Street, Santa Cruz, CA 95064*

⁴*Harvard-Smithsonian Center for Astrophysics, 60 Garden Street, Cambridge, MA 02138*

⁵*Department of Physics, University of California, 1156 High Street, Santa Cruz, CA 95064*

⁶*Carnegie Observatories, 813 Santa Barbara Street, Pasadena, CA 91101*

⁷*Racah Institute of Physics, The Hebrew University, Jerusalem 91904, Israel*

Accepted 2012 May 4. Received 2012 April 4; in original form 2010 November 4

ABSTRACT

The definition of homology for single-component galaxies is clear, but for multi-component (luminous and dark matter) galaxies there is some ambiguity. We attempt to clarify the situation by carefully separating the different concepts of homology that have been used to date. We argue that the most useful definition is that a set of galaxies is homologous if they are the same in all respects up to a set of three dimensional scaling constants which may differ from one galaxy to the next. Noting that we are free to choose the dimensional constants, we find that a set of hydrodynamic simulated galaxy merger remnants is significantly closer to homologous when the dimensional length constant is taken to be the radius containing equal amounts of dark and baryonic matter rather than the usual observationally motivated choice of the baryonic half-mass radius. Once the correct dimensional scaling constants are used, the stellar velocity dispersion anisotropy is essentially the sole source of the variation in the kinematic structure of these simulated merger remnants. In order to facilitate the use of these scaling constants to analyse observed galaxies, we calculated the relationship between our preferred dimensional scaling constants and the typical observationally accessible quantities.

1 INTRODUCTION

To what extent are galaxies (or some subset of galaxies) homologous in the sense that all individual objects are scaled copies of one another? The discovery of the Fundamental Plane (FP) (Djorgovski & Davis 1987; Dressler et al. 1987) of elliptical galaxies distinctly sharpened this question because galaxies showed a regularity that almost, but not quite, followed that expected from the virial theorem for systems in dynamical equilibrium. The virial theorem holds regardless of whether galaxies are homologous, but if each galaxy were unique, then the FP would have a large scatter. If all galaxies were simply scaled copies of one another, then the FP would follow the virial expectation. In either of these cases, the FP would likely not have generated the interest that it has because it would either be less useful (in the former case) or less interesting (in the latter case). Actual galaxies seem to be in between these two possibilities: they are quite regular in structure, but do not quite follow the simple virial expectation. An understanding of the origin of the FP requires at least one ingredient aside from the virial theorem, and the search for that missing ingredient has been the focus of a great number of observational and theoretical studies.

Homology means that all galaxies are somehow scaled copies of one another. Obviously the property of homology

applies only to a set of objects, not to individual galaxies. If galaxies were made up of only one type of matter, then there is no ambiguity in the definition of homology. However, they are in fact made up of dark matter, luminous matter, and gas, the behaviour of each component is dominated by different physics, and the components are only weakly coupled. For such systems, the proper definition of homology is not clear. Several informal definitions seem to be in common use; for single component systems, all of these definitions are equivalent. Not so for multi-component galaxies.

We formalize the definitions currently in use and discuss which definitions are stronger or weaker in the sense that the galaxies that fit one definition are or are not a subset of those that fit another definition. Then we apply these ideas to galaxy remnants produced in numerical simulations. Finally, we discuss how these ideas may be applied to observed galaxies.

It is obviously the case that homology can only apply to some subset of galaxies (ellipticals and spirals are quite distinct). It has also been established that even for restricted sets of galaxies, homology can only be approximate because, for example, the shape of the surface brightness as a function of radius (parametrized by the Sérsic parameter n) correlates with galaxy luminosity (Prugniel & Simien

1997). However, elliptical galaxies are still quite *close* to being homologous—close enough that the concept is still very useful.

In Section 2 we show that homology is closely related to the choice of units for each galaxy: homologous galaxies are all the same up to a choice of units, where the units are allowed to change from one galaxy to the next. For multi-component galaxies, there is an ambiguity in the definition of homology that we may be able to exploit: perhaps the baryonic half-light radius is not the right choice to make all galaxies look the same. In Section 3 we review recent observational and theoretical work on the subject of galaxy structure and homology. In Section 4 we use numerical simulations of galaxy mergers to show that there is indeed a better choice of dimensional scaling constants, at least for the set of simulations under consideration. Unfortunately our preferred choice of scaling constants are not directly observationally accessible, so in Section 5 we work out the relationship between our preferred definition of the scaling constants and the conventional choices for plausible baryonic and dark matter distributions. Finally, in Section 6 we summarize our conclusions.

2 THEORETICAL PRELIMINARIES

When discussing single-component models, it is fairly clear how to make the definition of homology precise. Such a galaxy is fully described by its distribution function $f(\mathbf{x}, \mathbf{v})$ giving the density of stars with the given position \mathbf{x} and velocity \mathbf{v} . A set of galaxies is homologous if there exists a ‘master’ distribution function F where the distribution function of a specific galaxy f is obtainable from F via:

$$f(\mathbf{x}, \mathbf{v}) = \frac{M}{R^3 V^3} F(\mathbf{x}/R, \mathbf{v}/V) \quad (1)$$

where R , V , and M are arbitrary scale constants, different for each galaxy. If one knows the universal distribution function, three numbers suffice to completely describe a galaxy. This will be called *scaling homology*.

Scaling homology is closely related to systems of units. It means that all galaxies are the same if one works with the correct system of units, where the units are allowed to change from galaxy to galaxy.

It is very important to recognize at this point that these scaling constants are *not* necessarily equal to the half-mass radius, the velocity dispersion, and the total galaxy mass. For single component galaxies, these choices for the scaling constants are essentially the only reasonable ones: if galaxies are homologous, then other choices will end up being simple functions of the half-mass radius, etc. However, for multi-component galaxies, our job is to take a set of galaxies and *infer* the definitions for R , V , and M that make all of their distribution functions derivable from a single ‘master’ distribution function. If no such definition exists, then the galaxies are not scaling-homologous. Section 4 is devoted to carrying out this analysis for a set of simulated galaxy merger remnants.

Perhaps the most common method of defining homology is to define structure constants relating the true values of a galaxy’s mass and luminosity to ‘virial estimates’ obtained using scaling constants. From Bender et al. (1992):

$$L = c_1 I_{\text{eff}} r_{\text{eff}}^2 \quad (2)$$

$$M = c_2 \sigma_0^2 r_{\text{eff}} \quad (3)$$

where L is the galaxy’s luminosity, M is the mass, r_{eff} is the projected half-light radius, I_{eff} is the mean surface brightness inside r_{eff} , σ_0 is the projected aperture velocity dispersion, and c_1 and c_2 are structure constants defined by these two equations. The important point is that M is the true mass of the galaxy while σ_0 and r_{eff} are scale factors combined in such a way as to dimensionally produce a mass (up to physical constants). Therefore variation of c_2 from galaxy to galaxy indicates that mass profiles of the two galaxies differ to produce a different relationship between the virial estimator and the actual mass. A set of galaxies is said to be homologous if these structure constants are the same for all galaxies. We denote this definition *structure-constant homology*.

It is easy to show that for single-component systems, structure-constant homology and scaling homology are equivalent. Putting the two definitions into the same language, we have:

$$\rho(\mathbf{x}) = \int f(\mathbf{x}, \mathbf{v}) d^3 \mathbf{v} \quad (4)$$

the total kinetic energy is

$$\text{KE} = \frac{1}{2} \int |\mathbf{v}|^2 f(\mathbf{x}, \mathbf{v}) d^3 \mathbf{x} d^3 \mathbf{v} \quad (5)$$

and the total potential energy is:

$$\begin{aligned} \text{PE} &= -\frac{G}{2} \int \frac{\rho(\mathbf{x})\rho(\mathbf{y}) d^3 \mathbf{x} d^3 \mathbf{y}}{|\mathbf{x} - \mathbf{y}|} \\ &= -\frac{G}{2} \int \frac{f(\mathbf{x}, \mathbf{v})f(\mathbf{y}, \mathbf{w}) d^3 \mathbf{x} d^3 \mathbf{y} d^3 \mathbf{v} d^3 \mathbf{w}}{|\mathbf{x} - \mathbf{y}|} \end{aligned} \quad (6)$$

where G is Newton’s gravitational constant. The scalar virial theorem is then:

$$\begin{aligned} &\int |\mathbf{v}|^2 f(\mathbf{x}, \mathbf{v}) d^3 \mathbf{x} d^3 \mathbf{v} \\ &= \frac{G}{2} \int \frac{f(\mathbf{x}, \mathbf{v})f(\mathbf{y}, \mathbf{w}) d^3 \mathbf{x} d^3 \mathbf{y} d^3 \mathbf{v} d^3 \mathbf{w}}{|\mathbf{x} - \mathbf{y}|}. \end{aligned} \quad (7)$$

Let us define three arbitrary scaling constants R , V , and M , and dimensionless coordinates $\tilde{\mathbf{x}} = \mathbf{x}/R$ and $\tilde{\mathbf{v}} = \mathbf{v}/V$.

$$\begin{aligned} &R^3 V^5 \int |\tilde{\mathbf{v}}|^2 f(\mathbf{x}, \mathbf{v}) d^3 \tilde{\mathbf{x}} d^3 \tilde{\mathbf{v}} \\ &= \frac{G R^5 V^6}{2} \int \frac{f(\mathbf{x}, \mathbf{v})f(\mathbf{y}, \mathbf{w}) d^3 \tilde{\mathbf{x}} d^3 \tilde{\mathbf{y}} d^3 \tilde{\mathbf{v}} d^3 \tilde{\mathbf{w}}}{|\tilde{\mathbf{x}} - \tilde{\mathbf{y}}|} \end{aligned} \quad (8)$$

Using the definition of the dimensionless distribution function in Equation 1, the virial theorem becomes:

$$\begin{aligned} &M V^2 \int |\tilde{\mathbf{v}}|^2 F(\tilde{\mathbf{x}}, \tilde{\mathbf{v}}) d^3 \tilde{\mathbf{x}} d^3 \tilde{\mathbf{v}} \\ &= \frac{G M^2}{2R} \int \frac{F(\tilde{\mathbf{x}}, \tilde{\mathbf{v}})F(\tilde{\mathbf{y}}, \tilde{\mathbf{w}}) d^3 \tilde{\mathbf{x}} d^3 \tilde{\mathbf{y}} d^3 \tilde{\mathbf{v}} d^3 \tilde{\mathbf{w}}}{|\tilde{\mathbf{x}} - \tilde{\mathbf{y}}|} \end{aligned} \quad (9)$$

Therefore we define the structure constants

$$\begin{aligned} \alpha &= \int |\tilde{\mathbf{v}}|^2 F(\tilde{\mathbf{x}}, \tilde{\mathbf{v}}) d^3 \tilde{\mathbf{x}} d^3 \tilde{\mathbf{v}} \\ &= \frac{1}{M} \int |\mathbf{v}/V|^2 f(\mathbf{x}, \mathbf{v}) d^3 \mathbf{x} d^3 \mathbf{v} \end{aligned} \quad (10)$$

and

$$\begin{aligned}\beta &= \int \frac{F(\tilde{\mathbf{x}}, \tilde{\mathbf{v}})F(\tilde{\mathbf{y}}, \tilde{\mathbf{w}}) d^3\tilde{\mathbf{x}} d^3\tilde{\mathbf{y}} d^3\tilde{\mathbf{v}} d^3\tilde{\mathbf{w}}}{|\tilde{\mathbf{x}} - \tilde{\mathbf{y}}|} \\ &= \frac{R}{M} \int \frac{f(\mathbf{x}, \mathbf{v})f(\mathbf{y}, \mathbf{w}) d^3\mathbf{x} d^3\mathbf{y} d^3\mathbf{v} d^3\mathbf{w}}{|\mathbf{x} - \mathbf{y}|}\end{aligned}\quad (11)$$

With these definitions, the virial theorem is simply:

$$\alpha V^2 = \beta \frac{GM}{2R} \quad (12)$$

and comparing to equation 3 reveals that:

$$c_2 = \left(\frac{2\alpha}{G\beta}\right) \left(\frac{M_{\text{bar}}}{M}\right) \left(\frac{R}{r_{\text{eff}}}\right) \left(\frac{V}{\sigma_0}\right)^2 \quad (13)$$

where M_{bar} refers to the total baryonic mass of the galaxy.

2.1 Two Component Galaxies

Describing a galaxy that contains both stellar and dark matter requires specifying two distribution functions, f and g , with corresponding dimensionless functions F and G .

Why do we use separate distribution functions for baryonic matter and dark matter, but we do not separate the different components of baryonic matter into young stars, old stars, disc stars, etc? The different stellar components have different formation histories and the moments of the distribution function that appear in the Jeans equations will be different for the different stellar components. Here we attempt to strike balance between accuracy and simplicity: our description of the system should be complex enough to be accurate, but simple enough to be informative. Hence we separate baryonic matter from dark matter because the two types of matter obey different physics and have *very* different histories. By including all baryonic matter in a single distribution function, we sacrifice some accuracy in order to make the description simple enough to be easily understood and manipulated.

Allowing for a second component, the virial theorem takes the form:

$$\begin{aligned}&\frac{2RV^2}{GM} \left(\int |\tilde{\mathbf{v}}|^2 F(\tilde{\mathbf{x}}, \tilde{\mathbf{v}}) d^3\tilde{\mathbf{x}} d^3\tilde{\mathbf{v}} + \int |\tilde{\mathbf{v}}|^2 G(\tilde{\mathbf{x}}, \tilde{\mathbf{v}}) d^3\tilde{\mathbf{x}} d^3\tilde{\mathbf{v}} \right) \\ &= \int \frac{F(\tilde{\mathbf{x}}, \tilde{\mathbf{v}})F(\tilde{\mathbf{y}}, \tilde{\mathbf{w}})}{|\tilde{\mathbf{x}} - \tilde{\mathbf{y}}|} d^3\tilde{\mathbf{x}} d^3\tilde{\mathbf{y}} d^3\tilde{\mathbf{v}} d^3\tilde{\mathbf{w}} \\ &+ 2 \int \frac{F(\tilde{\mathbf{x}}, \tilde{\mathbf{v}})G(\tilde{\mathbf{y}}, \tilde{\mathbf{w}})}{|\tilde{\mathbf{x}} - \tilde{\mathbf{y}}|} d^3\tilde{\mathbf{x}} d^3\tilde{\mathbf{y}} d^3\tilde{\mathbf{v}} d^3\tilde{\mathbf{w}} \\ &+ \int \frac{G(\tilde{\mathbf{x}}, \tilde{\mathbf{v}})G(\tilde{\mathbf{y}}, \tilde{\mathbf{w}})}{|\tilde{\mathbf{x}} - \tilde{\mathbf{y}}|} d^3\tilde{\mathbf{x}} d^3\tilde{\mathbf{y}} d^3\tilde{\mathbf{v}} d^3\tilde{\mathbf{w}}.\end{aligned}\quad (14)$$

We define

$$\begin{aligned}\gamma &= 2 \int \frac{F(\tilde{\mathbf{x}}, \tilde{\mathbf{v}})G(\tilde{\mathbf{y}}, \tilde{\mathbf{w}}) d^3\tilde{\mathbf{x}} d^3\tilde{\mathbf{y}} d^3\tilde{\mathbf{v}} d^3\tilde{\mathbf{w}}}{|\tilde{\mathbf{x}} - \tilde{\mathbf{y}}|} \\ &= \frac{2R}{M} \int \frac{f(\mathbf{x}, \mathbf{v})g(\mathbf{y}, \mathbf{w}) d^3\mathbf{x} d^3\mathbf{y} d^3\mathbf{v} d^3\mathbf{w}}{|\mathbf{x} - \mathbf{y}|}\end{aligned}\quad (15)$$

so that at last we have the virial theorem in the form:

$$(\alpha_f + \alpha_g)V^2 = (\beta_f + \beta_g + \gamma) \frac{GM}{2R}. \quad (16)$$

From these expressions it is clear that for multi-component galaxies:

- Scaling homology implies structure-constant homology.

- Structure-constant homology does not imply scaling-homology because structure-constant homology only requires a small number of constraints on the definite integrals defining α , β , and γ .

- A set of galaxies being structure-constant homologous does not imply that each component is separately structure-constant homologous. Structure-constant-homologous galaxies can be built from non-homologous components if the change in α_f compensates for the change in α_g and similarly for β .

- The components of galaxies being structure-constant-homologous does not imply that the galaxies are structure-constant-homologous.

- The structure constants for multi-component galaxies are not simply the sum of the structure constants of the individual components owing to the cross term γ .

Finally, similar considerations for scaling-homology yield:

- Scaling-homology of galaxies implies scaling-homology of the components.

- Scaling-homology of the components does not imply scaling-homology of galaxies. If a set of galaxies is composed of scaling-homologous components, then the set of multi-component galaxies will be scaling-homologous only if the ratios of the scaling constants for each component are the same for all of the galaxies in the set. That is, R_f/R_g must be the same for all of the galaxies.

One may wonder whether the dark and luminous components should be allowed their own scaling constants. This idea is problematic because scaling the components separately disturbs the dynamical equilibrium of the galaxy. Consider a galaxy in dynamical equilibrium where the baryonic scale radius is allowed to shrink to zero, making the baryons into a point mass. The dark matter far outside the original baryonic scale radius will not be significantly affected by this operation. However, the dark matter near the centre (inside the original baryonic scale radius) will have more mass enclosed after the change. The new galaxy will obviously be out of dynamical equilibrium.

We have seen from the above considerations that scaling homology is a stronger concept than structure-constant homology in the sense that scaling homology implies structure-constant homology, but not vice versa. For two-component galaxies, the two components can undergo compensating changes to leave the structure constants unchanged. This does not seem to be a desirable property for a concept like homology. Finally, there is a certain theoretical elegance to the viewing homology as closely connected to the choice of the system of units—a set of galaxies is scaling homologous if all of the galaxies are the same when using the correct system of units. For all of these reasons we advocate that homology be taken to mean scaling homology. Structure-constant homology should be clearly denoted as a different concept.

2.2 Tilt of the Fundamental Plane

There are three independent ways to generate the tilt in the fundamental plane. Any or all of them may be at work.

The first is a systematic change in the stellar mass-

to-light ratio with the mass of the host galaxy via trends in the age, metallicity, or initial mass function of the stellar population. In this case the stellar and dark matter distribution functions are scaling (and therefore structure-constant) homologous because the masses of stars and dark matter components are unaffected.

The second is a systematic change in the dark matter fraction near the centre of the galaxy. This is a mild form of non-homology which is achieved by changing the ratio of the mass scaling constants $M_{\text{bar}}/M_{\text{DM}}$ with galaxy mass, where M_{DM} is the total dark matter mass of the galaxy. Overall scaling- and structure-constant homology are violated, but the baryonic components by themselves may be nearly scaling- and structure-constant-homologous. Furthermore, as long as the stellar and dark matter remain nearly decoupled due to their very different half mass radii, then changing the dark matter fraction should not greatly disturb the dynamical equilibrium of the stellar material. In this case the stellar population mass-to-light ratio is identical for all galaxies, but the total mass-to-light (both for the entire galaxy and within any radius) ratio changes systematically with mass.

The third possibility is that homology is flagrantly violated and the baryonic components of galaxies are neither scaling nor structure-constant homologous. Even if the stellar population mass-to-light ratio is always the same, there is still total freedom in the total mass-to-light ratio owing to the total freedom in the choice of dark matter profile for each galaxy. It may change or be constant as a function of radius, and the total mass-to-light ratio may change or be constant for the entire set of galaxies.

A great source of confusion is that the first and second possibilities are very different theoretically but rather similar observationally. Everyone agrees that the first possibility involves homology and the third possibility involves non-homology. However, the second possibility is *observationally* very similar to the first possibility but *theoretically* very similar to the third possibility. This unfortunate circumstance makes it difficult to come to firm conclusions.

2.3 Variable dark matter fraction and equilibrium

There are two contributions to a total mass-to-light ratio: one from the characteristics of the stellar population and one due to the accompanying dark matter. If the mass-to-light ratio changes with galaxy mass because of a changing stellar population, then the FP will be tilted but the mass distribution may still be homologous. However, if the mass-to-light ratio changes due to changing dark matter fraction, then the galaxies *must* be non-homologous.

Consider the spherically symmetric Jeans equation (e.g. Binney & Tremaine 1987):

$$\frac{d \ln \nu}{d \ln r} + \frac{d \ln \sigma_r^2}{d \ln r} + 2\beta_a + \frac{1}{\sigma_r^2} \frac{d\Phi}{d \ln r} = 0 \quad (17)$$

where ν is the number density of tracer particles, σ_r is the radial component of the velocity dispersion, Φ is the total gravitational potential, $\beta_a = 1 - \sigma_\theta^2/\sigma_r^2$ is the anisotropy parameter, and σ_θ is the tangential component of the velocity dispersion.

The matter density is provided by two components, ρ_{bar} and ρ_{DM} for baryons and dark matter. The Poisson equation

is linear so the solutions obey the superposition principle. Putting this into the Jeans equation results in:

$$\frac{d \ln \nu}{d \ln r} + \frac{d \ln \sigma_r^2}{d \ln r} + 2\beta_a + \frac{1}{\sigma_r^2} \left(\frac{d\Phi_{\text{bar}}}{d \ln r} + b \frac{d\Phi_{\text{DM}}}{d \ln r} \right) = 0 \quad (18)$$

where Φ_{bar} and Φ_{DM} refer to the potential due to the baryonic and dark matter respectively and the constant b parametrizes the dark matter fraction. If a galaxy is in equilibrium for any value of b , then *any* change to b *must* be compensated by a change in the anisotropy β_a or a change in the radial fall-off of density or velocity dispersion.

Variations in the dark matter fraction and non-homology are the same concept. If the tilt in the FP is *not* due to systematic changes in the stellar population mass-to-light ratio, then it *must* be due to non-homology. There is no separate case where ‘only’ the dark matter fraction and therefore the observed mass-to-light ratios are changing.

2.4 What constitutes non-homology?

Given the somewhat confused use of the word homology in the present literature, it is perhaps easier to focus on what *non-homology* means. As discussed above, one way galaxies could be non-homologous is by having baryonic profiles that change shape from galaxy to galaxy. The fact that not all galaxies have the same Sérsic index already tells us that the population of galaxies cannot be perfectly homologous. If the dark and luminous components scale separately from each other so that different galaxies have different amounts of dark matter within some radius, then the galaxies *must* also be considered non-homologous.

Finally, recall that since structure-constant homology only places a few constraints on the definite integrals defining α , β , and γ , the luminous and dark components of a set of galaxies can undergo compensating changes so that the galaxies *would* be deemed structure-constant homologous, but would *not* be scaling homologous. We use this observation to argue that scaling homology is the more useful concept and the concept of structure-constant homology should be avoided.

3 RECENT WORK

Armed with a precise definition of the different flavors of homology we highlight a few recent observational and theoretical results. We wish to give a brief overview of the state of the field, but unfortunately none of these studies will be directly relevant to the present one because they all use the half-light radius as the relevant length scale. In section 4 we will show that for a large set of hydrodynamic simulations, we obtain more instructive results by using r_{eq} , the radius where the enclosed dark matter and luminous matter are equal. Simulated merger remnants look significantly more homologous when using r_{eq} than when using r_{eff} .

Thus far we have been concerned only with theoretical galaxies: all quantities of interest can be measured to arbitrary precision. However, the only observationally accessible quantities are projected ones. The measured mean surface brightness within the effective radius involves an integral along the light of sight and therefore implicitly mixes information about the entire mass/light profile at all radii.

Furthermore, both dark matter and stellar populations contribute to the measured mass-to-light ratios of galaxies. Variations of mass-to-light ratios due to one or the other of these possibilities are very different theoretically, but observationally similar.

One may ask if we could take the results of an observational or theoretical study discussed below, take a guess at the scaling of the density profile between r_{eq} and r_{eff} , and then directly compare the results of previous studies to our own. Unfortunately, carrying out such a project would tell us something about our assumed scaling between r_{eff} and r_{eq} , but it would not tell whether other authors would reach different conclusions if they use r_{eq} instead of r_{eff} . In order to answer the latter question, we need access to the full density profiles as a function of radius in the case of numerical studies. We unfortunately must wait for other groups to analyse their simulations in terms of r_{eq} in order to see if our findings hold true beyond our present set of simulations.

3.1 Observational Studies

There has been some success in recent years indicating that stellar population models have progressed to the point where it is possible to measure stellar mass-to-light ratios from spectra (e.g. Graves & Faber 2010). The usual assumption is that the initial mass function is universal, but recent observations have cast doubt on that idea (van Dokkum & Conroy 2011; Cappellari et al. 2012). Furthermore, in spite of the many codes available to estimate stellar masses (e.g. Bell et al. 2003; Kauffmann et al. 2003; Gallazzi et al. 2005; Blanton & Roweis 2007), many are based on a rather small number of libraries of stellar spectra (e.g. Bruzual & Charlot 2003). Thus one may be concerned about covariance between the different estimates of stellar mass because their fundamental assumptions are similar. If this is the case, then agreement between the different estimates indicates that their assumptions are similar, not that the stellar masses have actually been accurately measured.

Cappellari et al. (2006) used Schwarzschild (1979) modeling of SAURON (Bacon et al. 2001) early-type galaxies to show that the so-called virial mass estimator ($5r_{\text{eff}}\sigma^2/G$) is an excellent estimator of the dynamical mass within one effective radius. The SAURON survey also has stellar spectra over the whole galaxy image out to approximately one effective radius, and is thus excellently placed to use stellar population synthesis to finally break the degeneracy between dark matter fraction and stellar population mass-to-light ratio. Their Figure 17 unfortunately does not permit a single firm conclusion. For dynamical mass-to-light ratios below 2.8, there is a linear relationship between the stellar mass-to-light ratio and the dynamical mass-to-light ratio, indicating that the dark matter fraction does not change. For larger mass-to-light ratios, there is essentially a single stellar mass-to-light ratio, independent of the dynamical mass-to-light ratio, indicating that either the initial mass function or the dark matter fraction *does* change.

Bolton et al. (2008) and Koopmans et al. (2009) used strong gravitational lenses to argue that if one replaces the luminosity surface density in the FP with the mass surface density, one gets an untilted fundamental mass plane that is in full agreement with the virial expectation. Therefore the tilt in the FP must be due to variations in mass-to-light

ratio. However, there is little guidance from strong gravitational lensing about whether the total mass-to-light variation is due to changing dark matter fractions, changing stellar populations, or a changing initial mass function.

Taylor et al. (2010) used SDSS data to compare stellar mass and dynamical mass estimates for a set of galaxies. They found that the two were related, but non-linearly, and that the non-linearity could be removed by defining a ‘structure-corrected’ dynamical mass that takes the Sérsic parameter n of the galactic light into account. Thus they conclude that elliptical galaxies are not homologous. Taylor et al. (2010) made the conventional choice of scaling different galaxies by their half-light radii and central velocity dispersion in order to evaluate the question of whether or not they are homologous.

Graves & Faber (2010) study stacked SDSS spectra of early-type galaxies as a function of their position in the Fundamental Plane. They found that the variation in the dynamical mass-to-light ratios was too large to be explained by variations in the stellar mass-to-light ratios alone. This indicates varying dark matter fractions and is interpreted as non-homology in the galaxy population.

Auger et al. (2010) used multi-band Hubble Space Telescope images to construct stellar masses from stellar population models for 73 massive early-type galaxies identified as strong gravitational lenses as part of the SLACS survey (Czoske et al. 2008). Combining this information with velocity dispersions from the Sloan Digital Sky Survey (SDSS) (York et al. 2000), they concluded that the central dark matter fractions of massive early-type galaxies increase systematically with galaxy mass if one assumes a universal initial mass function. They found that the stellar mass-to-light ratio was essentially constant with galaxy mass. Barnabè et al. (2011) carried out dynamical modeling of a subset of these galaxies using ground-based integral-field-unit data and reached the same conclusion.

Grillo (2010) analyzed SDSS velocity dispersions along with stellar masses obtained from the JHU/MPA value-added galaxy catalog.¹ Dynamical considerations led them to conclude that the ratio of dynamical mass to dark mass was constant and they argued that the tilt of the FP is entirely due to stellar population effects. Grillo & Gobat (2010) used Schwarzschild (1979) models of 13 bright galaxies in the Coma cluster constructed by Thomas et al. (2007, 2009) along with stellar masses from SDSS to reach the same conclusion.

After many years of effort, it seems that stellar population modeling and dynamical modeling have progressed to the point where it is possible to separate the effects of changing dark matter fractions from that of changing stellar populations. However, recent studies have concluded both that galaxies are homologous and that they are not homologous. In addition, most applications of stellar population modeling require the assumption of a universal initial mass function. However, work by van Dokkum & Conroy (2011) and Cappellari et al. (2012) have cast doubt on this long-held assumption. If the initial mass function is truly not universal, both dynamical modeling and stellar population modeling will be more difficult.

¹ <http://www.mpa-garching.mpg.de/SDSS/>

3.2 Theoretical Studies

González-García & van Albada (2003) and Boylan-Kolchin et al. (2005) studied dissipationless merger simulations to determine whether mergers leave the FP intact. González-García & van Albada (2003) started with structure-constant homologous systems and found that their remnants did not share the property. The merger remnants *do* lie on the FP, evidently because the two structure constants are able to undergo compensating changes since they only appear in a multiplicative combination in the FP relation (their Equation 6). Boylan-Kolchin et al. (2005) studied a smaller number of much higher resolution simulations and found that both structure-constant homology and the FP were preserved by the merger process at the 10% level. They did, however, find a significant violation of homology for radial-orbit mergers.

Dekel & Cox (2006) used numerical simulations to study dissipation as the potential origin of the FP tilt. They assumed that all observable galaxy properties are power-law functions of the mass of the galaxy and the gas fraction, and then used several merger simulations with different gas fractions and masses in order to fix the power-law exponents and constants in their model. They were left with a set of constraints on the power-law exponents such that for any observed FP tilt, one could solve for the properties of the progenitor galaxies (e.g., gas fraction) as a function of mass. This of course depends on their merger simulations being good representatives of all mergers of that mass and gas fraction.

Robertson et al. (2006) used a large number of dissipational simulations of galaxy mergers, assumed a constant stellar mass-to-light ratio and concluded that with a sufficient amount of gaseous dissipation, merger remnants naturally produce a tilted FP. Since they assumed a constant stellar mass-to-light ratio, this tilt must have been caused by structural non-homology/varying dark matter fraction.

Hopkins et al. (2008) performed an extensive study of dissipation and the origin of the fundamental plane. They seem to be concerned with structure-constant homology, but dismiss non-homology as the source of the FP tilt. They assert that gas dissipation causes a varying dark-matter fraction inside the effective radius, which in turn tilts the FP. As stated above, we note that a varying dark-matter fraction is not distinct from non-homology. However, it can perhaps be considered to be a weak form of non-homology where only one of many possible degrees of freedom is exercised.

3.3 Relation to the present study

It is conceivable that any or all of these studies would reach a different conclusion if they were to use our definition of length, velocity, and mass scales rather than the usual observationally motivated definitions. In order to make this determination, we need more information than is available in the published papers, so we must wait for other groups to try analyzing their simulations and observations in terms of r_{eq} rather than r_{eff} .

We hasten to add that we are *not* claiming that any previous authors have made any mistake. Other researchers have correctly formulated and answered questions about the scaling relations of galaxies. Given the assumption that the relevant length scale was the baryonic half-mass radius,

these studies generally found measurable non-homology in the galaxy population that manifested itself by a changing central dark matter fraction.

We are pointing out that the choice of r_{eff} as the relevant length scale is arbitrary, and other choices may be more instructive in understanding galaxies and galaxy merger remnants. On the bases of our simulations, we have found that scaling the simulations by r_{eq} gives very instructive results. We hope that other researchers will find this terminology similarly useful.

4 APPLICATION TO SIMULATIONS

As already noted, the dimensional scaling constants used in the definition of scaling-homology are *not* required to be the conventional choices of half-mass radius, central velocity dispersion, etc. In this section we consider a set of simulated galaxy merger remnants and search for a definition of the dimensional scaling constants so that the dimensionless properties of the set of remnants are as similar as possible.

Once one has arrived at a definition for the scaling constants that seems to work well, one must compute the value for a given galaxy. Therefore we are restricting ourselves to simple, physically-motivated definitions of the dimensional scaling constants, such as the baryonic half-mass radius, the total half-mass radius, the radius where the enclosed baryonic and dark masses are equal, etc.

One could imagine carrying out a high-dimensional minimization where the function to be minimized is the sum of the total deviations of the scaled density and velocity profiles from the mean scaled profiles for all galaxies. The free parameters in the minimization are the three scaling constants for each galaxy. This would effectively tell you whether or not there *exists* a definition of the scaling constants that makes the galaxies scaling-homologous. However, it would *not* give a simple way to compute the dimensional scaling constants for a *given* galaxy. One would *know* the value of the scaling constants for a galaxy in the ‘training’ set: the fitting procedure would provide it. But one would not be able to compute the dimensional constant for a *new* galaxy, not in the training set.

Using numerical simulations allows us to quickly explore many possible definitions of the scaling constants with little uncertainty in, for example, the total galaxy mass or velocity dispersion. The simulated galaxies are of course imperfect stand-ins for actual galaxies, but our hope is that working with simulated galaxies will allow us to eliminate many of the definitions that are possible and focus on one (or a few) that seem to work well. Only the most successful choices when compared to simulations will be considered including the additional complications inherent to observational data.

There are two sets of simulations of binary mergers considered here. The *Sbc* series consists of equal mass mergers between two identical gas-rich progenitors on a variety of orbits. The *G* series consists of mergers of galaxies with lower gas fractions and a wide range mass ratios using only a few different orbits. Cox et al. (2006) contains a full description of the simulations.

We considered eight possible radius scales including stellar, dark, and total 3D effective radii and projected effective radii, the radius where stellar mass density and dark

mass density are equal, and finally the radius where the enclosed stellar mass and enclosed dark mass are equal. We evaluated thirty mass scales including the stellar, dark, and total mass, the total of each type of mass within each of four radii (stellar effective radius, dark effective radius, radius where stellar and dark densities are equal, and the radius where the enclosed stellar and dark masses are equal), and the mass scale that sets each of the three types of mass density to one at each of the four radii. The last dimensional choice is either a velocity or a time, and we tried the central 3D velocity dispersion, the projected velocity dispersion, and dynamical times at each of the above listed radii.

Evaluating one ‘model’ requires a choice of one of each of the three dimensional constants: length, mass, and velocity/time. This leads to a very large number of combinations. Fortunately, only a few choices work better than the conventional observationally motivated choices of baryonic half-mass radius, central velocity dispersion, and total baryonic mass. In this paper we plot only the conventional choices and the best alternate definition we found: the length scale is r_{eq} , the radius such that the enclosed dark and baryonic matter are equal, M_{eq} , the mass enclosed within r_{eq} , and t_{eq} , the dynamical time at r_{eq} . For the dynamical time, we use

$$t_{\text{dyn}} = \sqrt{\frac{3\pi}{32G\rho}} \quad (19)$$

so that

$$t_{\text{eq}} = \sqrt{\frac{\pi^2 r_{\text{eq}}^3}{8GM_{\text{eq}}}}. \quad (20)$$

To evaluate each choice of the scale constants, we plot dimensionless density and velocity dispersion profiles for all galaxies:

$$\tilde{\rho}(r) = \frac{R^3 \rho(r/R)}{M} \quad (21)$$

$$\tilde{\sigma}(r) = \frac{\sigma(r/R)}{V} \quad (22)$$

where r is the magnitude of the radius vector.

For simplicity we use spherical apertures to convert the 3D density and velocity profiles of the simulated galaxies into the 1D profiles shown here. Using ellipsoidal profiles instead does not change our conclusions. The velocity dispersion and rotation information is given in spherical coordinates r, θ , and ϕ where ϕ is the azimuthal angle and the coordinate system is defined by the shape of the stellar remnant so that the z axis corresponds to the short axis of the remnant.

If the simulated galaxies are perfectly scaling-homologous and we have hit upon the correct definition of the dimensional scaling constants, then the dimensionless density and velocity dispersion profiles will be exactly the same for all galaxies. Non-scaling-homologous galaxies will lead to large variations in the profiles from galaxy to galaxy. Therefore we plot the dimensionless profiles for *all* galaxies (with some transparency in each line so that the effects of over-plotting are minimized) and seek the definition of scaling constants that leads to the least variation from galaxy to galaxy.

For each simulation, we must estimate various observationally relevant quantities from simulation snapshots. For

real galaxies, observables such as the half-light radius, aperture velocity dispersion, and luminosity are affected by star formation history, age gradients, metallicity gradients, and dust. We ignore the majority of these complications and make simple assumptions that allow us to focus on the essential physics that determine the structure of merger remnants. In the future, a more detailed study using a code that allows us to take the effects stellar populations and dust into account (e.g. Jonsson 2006; Jonsson et al. 2010) would be worthwhile.

For the moment, we assume a constant stellar mass-to-light ratio and no dust scattering or absorption allowing for a simple relationship between mass and light. To estimate 3D and aperture velocity dispersions, we perform a maximum likelihood fit of a Gaussian distribution to the simulation particle velocities. The stellar remnants are very close to oblate spheroids, so to estimate the projected half-light radius we use a ‘‘typical’’ viewing angle 45 degrees between the pole-on and face-on views. We fit an ellipse to the projected iso-density contours and use the geometric mean of the semi-major and semi-minor axes as the half-light radius.

Figure 1 shows the dimensionless density profiles for the usual choice of the stellar effective radius for the length scale and the total stellar mass for the mass scale.

Figure 2 shows a different choice of length and mass scales. The length scale is r_{eq} , the radius at which the enclosed stellar and dark masses are equal, and the mass scale is the stellar mass enclosed within r_{eq} . In comparing to the mass profiles shown in Figure 1, we must ensure that the same physical radial range of the galaxies are probed. Multiplying the chosen units by a factor common to all galaxies does not change the result, so we normalize to the *Sbc201a-u4* simulation. For this simulation, $r_{\text{eff}} = 0.437r_{\text{eq}}$ and $M_{\text{bar}} = 1.54M_{\text{eq}}$.

The simulated galaxy merger remnants analysed here are not perfectly scaling-homologous. This is clear as soon as one realizes that the central slopes of the dark matter profiles are different between the G and *Sbc* series of simulations. Changing the scale radius can only shift curves from side-to-side in Figures 1 and 2; it cannot change the slopes. Even so, the radius and mass scale choice made in Figure 2 represents an impressively high degree of regularity among galaxy merger remnants given the variation in mass ratios, orbits, and gas fractions.

The total mass density profile for all of the simulations is very close to an isothermal $\rho \propto r^{-2}$ profile. This is in good agreement with recent studies of the mass profiles of elliptical galaxies using strong and weak gravitational lensing (Gavazzi et al. 2007, 2008; Bolton et al. 2008), dynamical studies of the line-of-sight velocity profiles of giant elliptical galaxies (Gerhard et al. 2001), and studies of the density and temperature profiles of x-ray gas in elliptical galaxies spanning a wide range in mass (Humphrey & Buote 2010).

Table 1 lists the RMS variation among all simulations for each physical quantity considered in this section. We take the value of the non-dimensional quantity under consideration at the appropriate scale radius (either r_{eff} or $0.437r_{\text{eq}}$) and compute the RMS variation of the resulting set of numbers. This serves as an indication of the galaxy-to-galaxy variation of, for example, the density profiles after applying a given set of scaling constants, and therefore of the utility of that particular set of scaling constants.

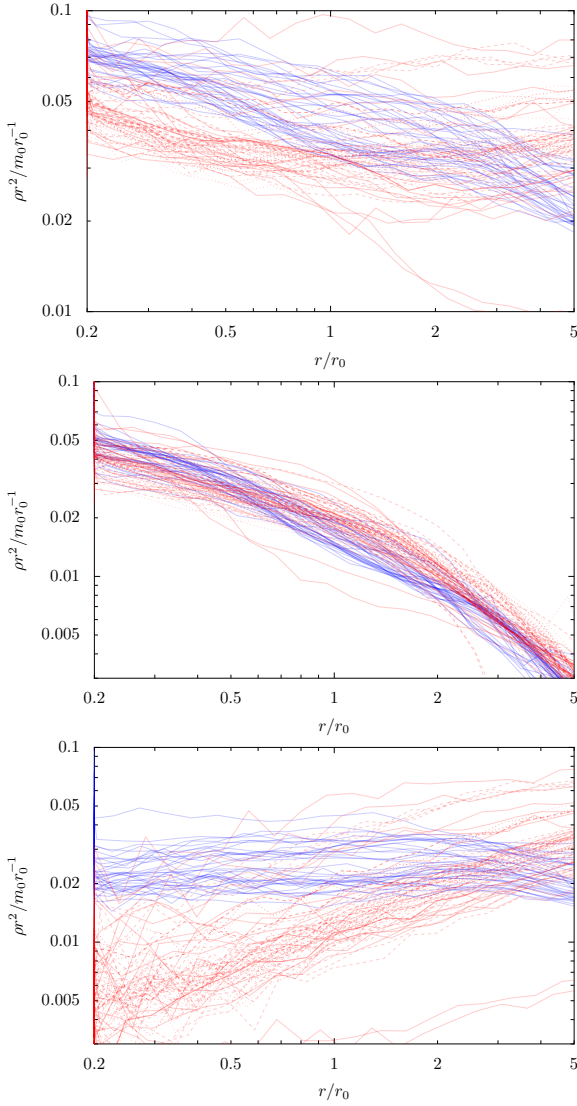


Figure 1. The dimensionless mass density profiles for all *G* and *Sbc* series simulations using the typical observationally motivated choices of stellar half mass radius and stellar mass for the length and mass scales. Blue lines are for *Sbc* simulations (with gas rich progenitors) while red lines are *G* series simulations. From the top, the total mass density, the stellar mass density, and the dark matter mass density. All mass profiles have been multiplied by r^2 to flatten them out. The stellar components of all of the simulations are strikingly similar. However, the chosen mass and length scales have nothing to do with the dark matter, so there is significant variation among the dark matter profiles of the different simulations. There is also a systematic change in the slope of the dark matter profiles between *Sbc* and *G* series simulations. No change of units will remove this difference.

Figure 3 shows remnant stellar velocity profiles for the typical choice of scaling constants: the stellar half-mass radius and the central projected velocity dispersion within $r_{\text{eff}}/8$. Figure 4 shows stellar velocity profiles when scaled by r_{eq} and the dynamical time at r_{eq} .

The velocity dispersion anisotropy profiles provide a convenient limit on the extent to which the velocity structure of the simulated remnants can be brought into a common system. The anisotropy is dimensionless, hence the

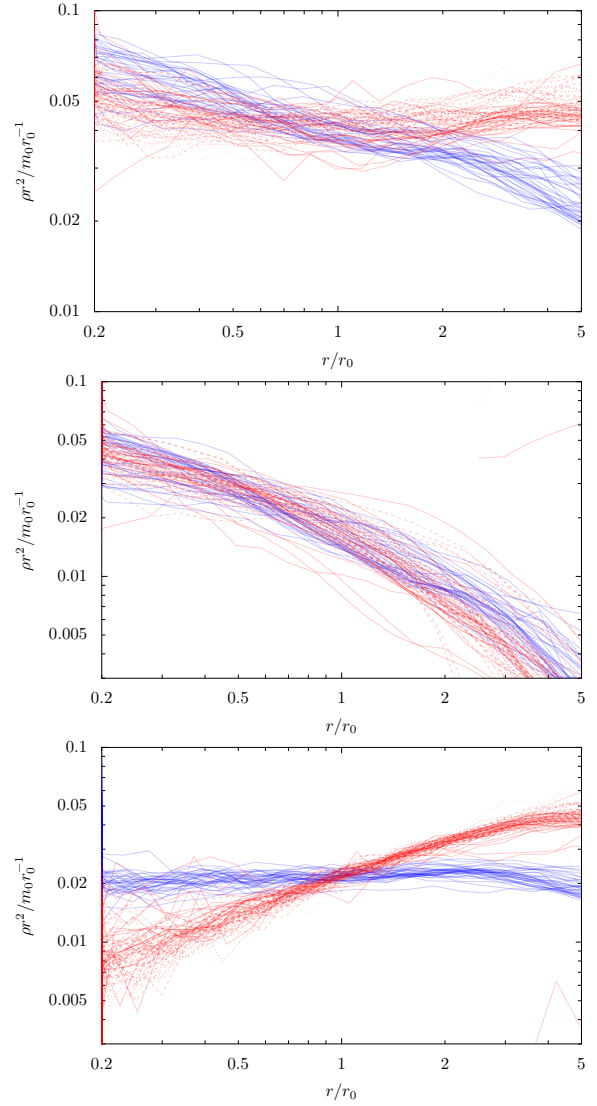


Figure 2. The dimensionless mass density profiles for all *G* and *Sbc* series simulations using our preferred choice of radius scale of $0.437r_{\text{eq}}$, where r_{eq} is the 3D radius where the enclosed stellar mass and dark mass are equal, and the mass scale is the 1.54 times the stellar mass enclosed within r_{eq} . The factors of 0.437 and 1.54 are chosen to ensure that these plots cover nearly the same physical region of the galaxy as Figure 1. With this choice of length and mass scale, the merger remnants show remarkable regularity. The dark matter mass profiles show 6% root-mean-square variation near the half-mass radius and the baryonic mass profiles show 17.7% RMS variation (compared to 51% and 18.5% respectively for the conventional observationally motivated set of scaling constants) in spite of the wide range of masses, gas fractions, orbits, and feedback recipes employed in these simulations.

only choice to be made is the length scaling constant. The anisotropy β_a is usually defined for a spherically symmetric object. In that case, $\sigma_\theta = \sigma_\phi$ and $v_r = v_\theta = v_\phi = 0$. The merger remnants presented here are not spherically symmetric so we define

$$\beta_\theta = 1 - \sigma_\theta^2 / \sigma_r^2 \quad (23)$$

and

$$\beta_\phi = 1 - \sigma_\phi^2 / \sigma_r^2 \quad (24)$$

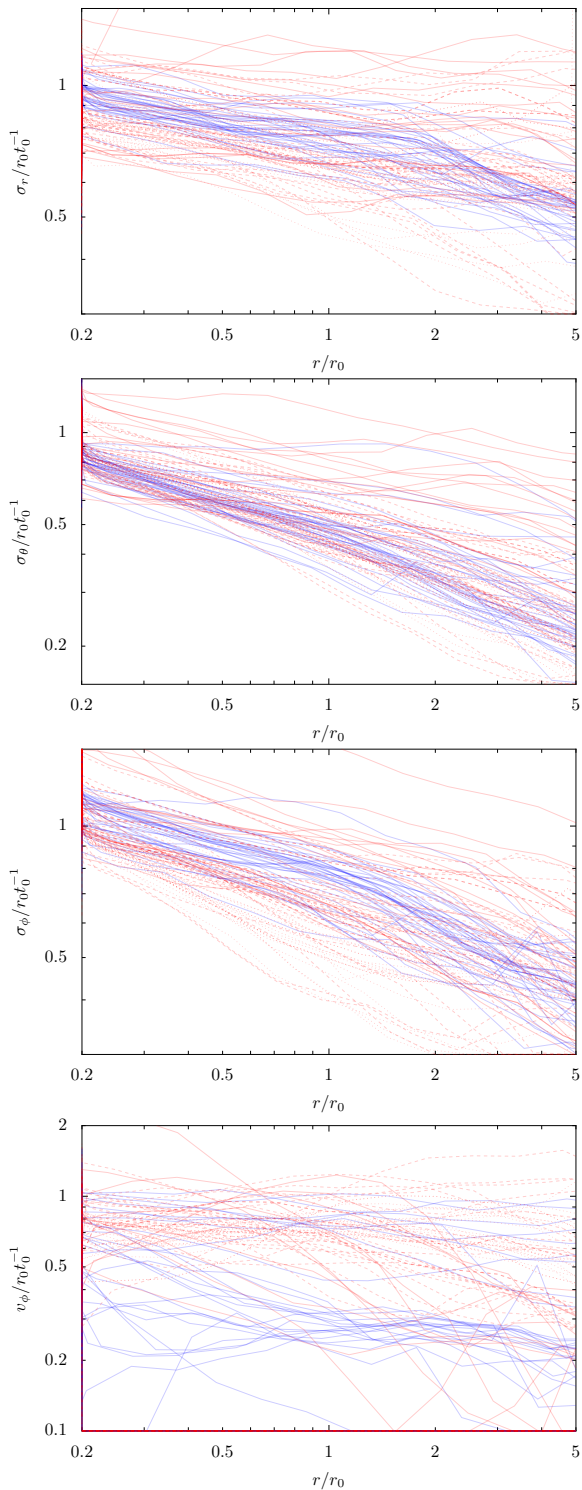


Figure 3. Dimensionless stellar velocity profiles with scale radius and velocity taken to be the usual observationally motivated ones: r_0 is the stellar half-mass radius and σ_0 is the projected velocity dispersion within an aperture of $r_{\text{eff}}/8$. From the top: 3D radial velocity dispersion, 3D velocity dispersion in the θ direction, 3D velocity dispersion in the azimuthal direction, and mean streaming velocity in the azimuthal direction. There is significant diversity in the velocity structure of simulated galaxy merger remnants.

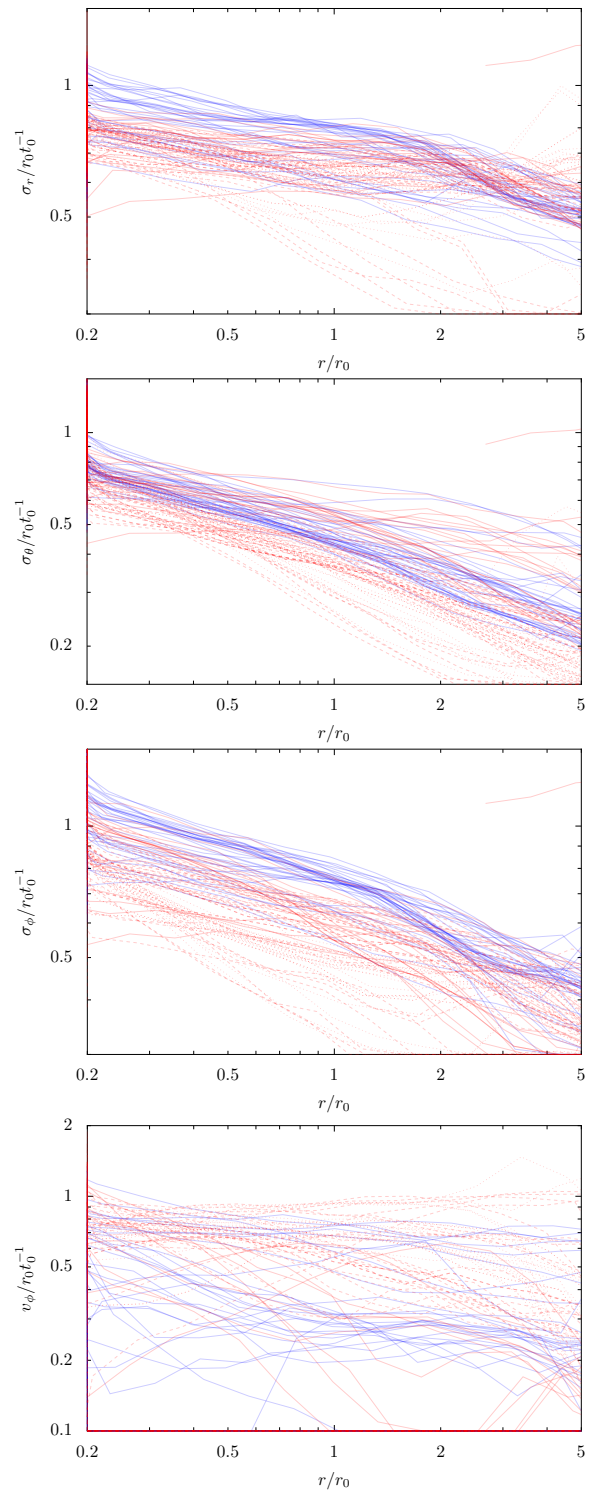


Figure 4. Dimensionless stellar velocity profiles with scale radius and time taken to be our preferred choices of r_{eq} and t_{eq} . This is an improvement over the conventional choices for scaling radius and velocity shown in Figure 3: the root-mean-square variation of σ_r , for example, at the scale radius goes from 27% to 15% in adopting the new set of scaling constants. The RMS variations of all quantities shown here are listed in Table 1.

Table 1. Root-mean-square variation of non-dimensional quantities among all simulations at the given scale radius. The conventional observationally-motivated choice of scaling constants is used for the column on the left (r_{eff} , M_{bar} , and σ_0), while our preferred choice of scaling constants based on the radius at which the enclosed dark and luminous masses are equal (r_{eq} , M_{eq} , and t_{eq}) is used for the column on the right. The quantities listed are the total mass density, the baryonic mass density, the dark matter mass density, the radial 3D stellar velocity dispersion, the 3D stellar velocity dispersion in the azimuthal direction, the 3D stellar velocity dispersion in the θ direction, the mean streaming velocity in the azimuthal direction, the specific kinetic energy of the stellar component, the specific kinetic energy of the dark matter component, the stellar velocity anisotropy in the azimuthal direction, and the stellar velocity anisotropy in the θ direction. All of the values are expressed as a percentage of the mean value for all galaxies except for the anisotropy β , where we do not divide by the mean because anisotropy is not positive definite.

Quantity	r_{eff} based scaling	r_{eq} based scaling
$\rho_{\text{bar}} + \rho_{\text{DM}}$	30.1%	10.1%
ρ_{bar}	18.5%	17.7%
ρ_{DM}	51.3%	6.04%
σ_r	26.9%	15.0%
σ_ϕ	37.6%	21.0%
σ_θ	40.8%	19.8%
v_ϕ	188%	176%
E_k/m (stars)	94.9%	11.0%
E_k/m (dark matter)	64.6%	14.1%
β_ϕ	0.263	0.238
β_θ	0.176	0.166

Figure 5 shows both β_θ and β_ϕ .

Virtually all of the remnants show stellar anisotropy profiles that rise with radius, in some cases to values near 1 (completely radial velocity dispersion). This is easily understood in terms of the dynamical origin of the stars at large radius in merger remnants (Dekel et al. 2005). Stars that end up at large radius are stars that were flung out from near the centre of mass when the merging galaxies underwent their first close pass. They have low angular momentum because they started out within approximately one effective radius, hence the anisotropy measured at large radius will be very radial.

The slopes of the anisotropy profiles are similar from galaxy to galaxy, but they are shallow. Changing the scale radius slides the curves horizontally, so any scale radius that would bring all the curves into agreement would be forced to vary dramatically from galaxy to galaxy.

We have seen that the density profiles of simulated remnants are remarkably consistent, but the velocity profiles show significant variation. Figure 5 suggests that the reason for the variation in the velocity profiles is the direction of the velocities of the stars. That is, there is a common *kinetic energy* profile, but the velocity profiles are different because some remnants are radially anisotropic, some are tangentially anisotropic, and some are rotating.

The specific kinetic energy is:

$$E_k/m = \frac{1}{2}(v_\phi^2 + \sigma_r^2 + \sigma_\theta^2 + \sigma_\phi^2) \quad (25)$$

where we have assumed Gaussian velocity distributions and

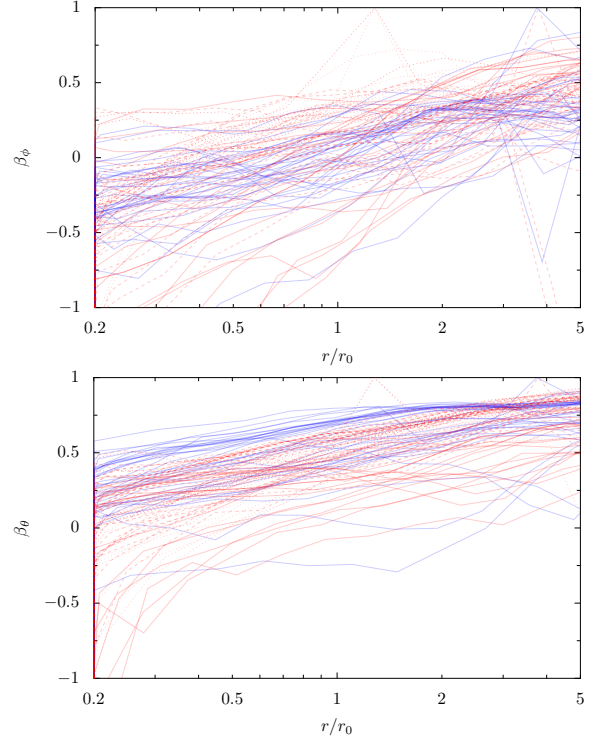


Figure 5. Stellar velocity dispersion anisotropy profiles for the usual choice of scale radius: the baryonic half-mass radius. This shows the reason why there is diversity in the velocity profiles of galaxy remnants in spite of the regularity in the density profiles. The virial theorem constrains the total kinetic energy of the system, but does not determine the *direction* of the velocities of the stars. Simulated remnants make use of this freedom and have a wide range of anisotropy profiles. Since the velocity anisotropy is dimensionless, changing dimensional scaling constants for each galaxy only moves each line horizontally. The shallow slope of the lines means that changing the definition of dimensional scaling constants cannot significantly change this plot to make the merger remnants more homologous.

neglected v_r and v_θ because the remnants are in steady-state.

Figure 6 shows kinetic energy profiles using the stellar half-mass radius and central projected velocity dispersion as scale constants. A common kinetic energy profile is not apparent with this choice of scale constants.

Figure 7 shows the dimensionless kinetic energy scaled by the mass-equality radius and the dynamical time at the mass-equality radius. The common energy structure of the merger remnants is apparent. In the case of the *Sbc* simulations there is as little as 3% RMS variation at the scale radius. There is again an offset between the two sets of simulations but nevertheless the lack of variation between simulations of a given set is remarkable.

It is clear that dark matter plays a significant but subdominant role in the dynamical equilibrium of the luminous parts of galaxies, and that the baryonic and dark matter components of galaxies scale very differently with radius. Observational and theoretical studies to date have almost exclusively used the classic observationally accessible half-light radius as the relevant scaling parameter to compare galaxies of different sizes and masses. However, the value

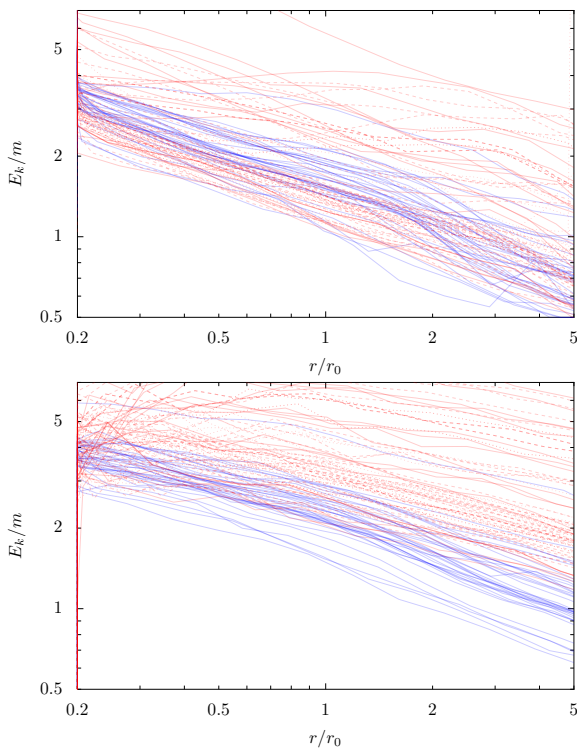


Figure 6. Specific kinetic energy profiles with scale constants r_0 equal to the stellar half mass radius and $t_0 = r_0/\sigma_0$. The upper panel shows the stellar component while the lower panel shows the dark matter component. There appears to be great diversity in the kinetic energy profiles of galaxy remnants.

of this parameter involves only the luminous matter. It is therefore quite plausible that adopting a different scaling radius will lead to different conclusions about homology: a set of galaxies (real or simulated) may be closer to homology when using r_{eq} as the scaling parameter.

Unfortunately it is very difficult to determine what conclusions other studies would have reached if they had used r_{eq} instead of r_{eff} without access to the full density and light profiles of the objects that were used in the study. One may be able to make reasonable extrapolations of the profiles from r_{eff} to r_{eq} , but this would not test the hypothesis. It is the conclusion of the present study that sets of galaxies may look more homologous or less homologous depending on the scaling radius that one uses, so making an assumption about the mass profiles in order to translate results from one radius to another would not test the hypothesis. One needs access to the full mass profile (in the case of simulated galaxies) or light profile (in the case of observational studies). On this point we hope that other observers and theorists use the relatively simple procedure of scaling by r_{eq} to see, first, if it makes their results easier to understand, and, second, if the results of our present study hold for broader sets of simulations and observations. We believe that adopting r_{eq} rather than r_{eff} would result in a significant gain in understanding.

5 OBSERVATIONAL IMPLICATIONS

As we have already mentioned, it is unfortunately the case that what we find to be the best definitions for the dimen-

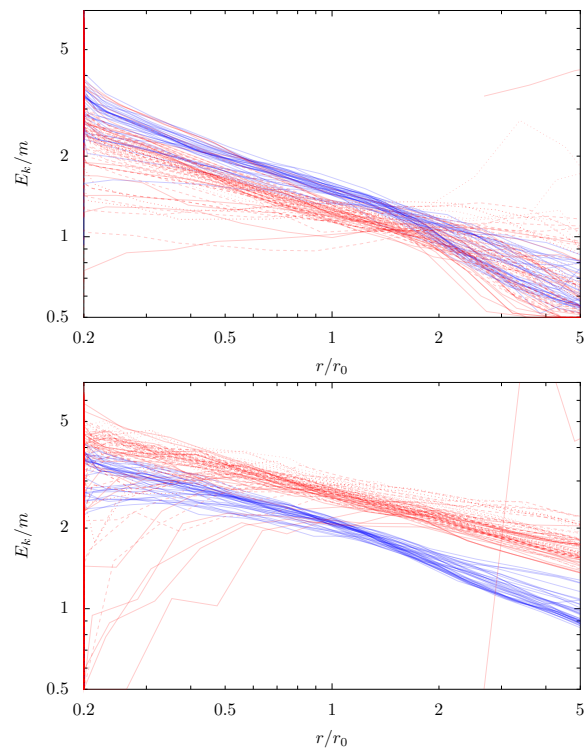


Figure 7. Specific kinetic energy profiles with scale constants taken to be our preferred choices of r_{eq} and the dynamical time at r_{eq} . The upper panel shows the stellar component and the lower panel shows the dark matter component. These kinetic energy profiles show very consistent behaviour given the great diversity of the origins of the remnants.

sional scaling constants that make simulated merger remnants close to homologous are not directly observable. In this section we define a plausible model for the density profiles of baryonic and dark matter in a two component galaxy and find the relationship between our preferred dimensional scaling constants and the observationally accessible values. That is, we find $r_{\text{eq}}/r_{\text{eff}}$ and $M_{\text{eq}}/M_{\text{bar}}$ for a range of plausible mass models.

It is possible to plot values of r_{eq} and M_{eq} for our simulated galaxy merger remnants but there are several problems with this idea. Most importantly, anyone who wished to use these values of r_{eq} and M_{eq} to interpret observations would automatically be subject to all of the uncertainties and deficiencies of numerical simulations, for example in the star formation law to name one issue among many. Second, because our galaxies *are* so close to homologous when r_{eq} is used as a scaling parameter, the values of $r_{\text{eq}}/r_{\text{eff}}$ and $M_{\text{eq}}/M_{\text{bar}}$ are nearly constant. Third, this particular set of simulated merger remnants do not span the full space of observationally relevant parameters, in the Sérsic index for example.

Therefore we seek a simple, easily understood, widely used, and observationally relevant mass model for which we can compute r_{eq} and M_{eq} . It is easy to understand the assumptions that enter such a model and, importantly, the model is not dependent on the details of our simulations even though the motivation to compute r_{eq} and M_{eq} arose from analysis of our simulations.

It is a relatively simple matter to calculate r_{eq} and M_{eq}

for any given combination of dark matter and baryonic mass profiles. We provide plots and fitting formulas for the most common cases in the hope that these formulas may be used in both observational and theoretical efforts to understand the scaling relations of galaxies. It is the conclusion of this study that different choices of the scaling parameters can lead to different conclusions about homology, so this is potentially an important point for both theoretical and observational studies of galaxy scaling relations.

For the baryonic component of our mass model, we use deprojected Sérsic profiles (Sérsic 1968):

$$I(r_p) = I_0 \exp \left[- \left(\frac{r_p}{r_s} \right)^{1/n} \right] \quad (26)$$

where I is the surface brightness, r_p is the projected radius, I_0 is the central surface brightness, and r_s is a scale radius chosen to ensure that the half-light radius is equal to some desired value. The Sérsic profile is defined for the projected surface brightness of a galaxy image. Approximations to the three-dimensional luminosity density that lead to the Sérsic profile under the assumption of spherical symmetry have been available for some time (Prugniel & Simien 1997; Lima Neto et al. 1999; Trujillo et al. 2002; Mamon & Lokas 2005). Exact analytic deprojections of the Sérsic profile for *integer values* of the Sérsic index n have also been available for some time (Mazure & Capelato 2002). Recently Baes & Gentile (2010) have generalized the Mazure & Capelato (2002) result for rational values of the Sérsic index, a very significant step forward for practical applications of the formulas since rational numbers can approximate any desired value arbitrarily well. These involve special functions, but numerical implementations of the necessary functions are available. Baes & Gentile (2010) also provide formulas for the case where the Sérsic index is real-valued rather than rational, but numerical implementations of the required special functions are not readily available. We use the Baes & Gentile (2010) formulas for exact deprojections of the Sérsic profile.

We allow two possibilities for the dark matter halo. The first is the familiar NFW formula (Navarro et al. 1996):

$$\rho(r) = \frac{\rho_{\text{NFW}}}{x(1+x)^2} \quad (27)$$

where ρ is the mass density, $x = r/r_{\text{NFW}}$, r_{NFW} is the scale radius where the profile switches from a logarithmic slope of -1 to -3, and ρ_{NFW} is a constant that sets the dark matter fraction of the galaxy as a function of radius.

There is good evidence from strong and weak gravitational lensing studies that the total mass density of elliptical galaxies is remarkably close to that of a singular isothermal sphere (SIS) over a large range in radii (Gavazzi et al. 2007, 2008; Bolton et al. 2008). Therefore the second possibility for the dark matter halo is the mass density such that the *total* mass density is given by:

$$\rho_{\text{T}}(r) = \frac{s^2}{2\pi G r^2} \quad (28)$$

where s parametrizes the depth of the potential well.

Figure 8 gives $r_{\text{eq}}/r_{\text{eff}}$ and $M_{\text{eq}}/M_{\text{bar}}$ for a range of models assuming an NFW halo parametrized by the shape of the baryonic mass profile and the dark matter fraction within one baryonic effective radius. For a fixed baryonic mass and effective radius, the dark matter fraction within one bary-

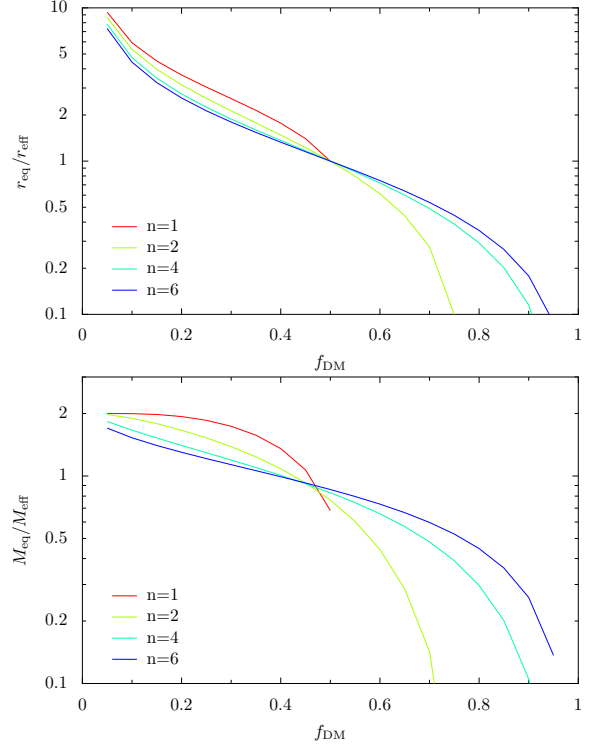


Figure 8. The relationship between our preferred dimensional scaling constants and directly observable quantities for a variety of mass models. The upper panel shows $r_{\text{eq}}/r_{\text{eff}}$ while the lower panel shows $M_{\text{eq}}/M_{\text{eff}}$, both as a function of the 3D dark matter fraction within the projected baryonic half-light radius. The parameter n is defined in equation 26 and gives the shape of the baryonic density profile. The dark matter fraction within one baryonic effective radius changes as a result of changes to the NFW density parameter ρ_{NFW} for a fixed baryonic model. The dominant consideration is the dark matter fraction, while the shape of the baryonic mass profile has a smaller effect.

onic projected half-light radius is adjusted by changing the NFW density parameter ρ_{NFW} . The results depend on the ratio of the $r_{\text{NFW}}/r_{\text{eff}}$ which indicates whether the density profile of the dark matter halo changes logarithmic slope near the baryonic component or far outside of it. The dependence is weak as long as $r_{\text{NFW}}/r_{\text{eff}}$ is sufficiently large, with the values of r_{eq} and M_{eq} approaching constant values. The plots and fitting formulas presented here assume $r_{\text{NFW}}/r_{\text{eff}} = 20$. The values of r_{eq} are $\sim 10\%$ smaller for $r_{\text{NFW}}/r_{\text{eff}} = \infty$ and $\sim 10\%$ larger for $r_{\text{NFW}}/r_{\text{eff}} = 10$, with little dependence on Sérsic index or central dark matter fraction. When $r_{\text{NFW}}/r_{\text{eff}}$ approaches unity, r_{eq} depends sensitively on the ratio, but that corresponds to halo concentrations $C = r_{\text{virial}}/r_{\text{NFW}}$ approaching 100, far outside the range predicted by simulations for main haloes (Bullock et al. 2001), although tidal stripping can lead to very large values of the concentration for sub-haloes (Diemand et al. 2008).

The value of r_{eq} for the case of an NFW halo may be approximated as:

$$\log_{10} \frac{r_{\text{eq}}}{r_{\text{eff}}} = \log_{10} f_1(f_{\text{DM}}) + f_2(f_{\text{DM}}) \log_{10}(n/3) + f_3(f_{\text{DM}}) \log_{10}^2(n/3) \quad (29)$$

Table 2. Fitting formula constants for NFW haloes.

Name	Value
k_1	1.183
k_2	0.7252
k_3	0.7241
k_4	0.5476
k_5	2.752
k_6	-0.1582
k_7	0.09714
k_8	-0.6602
k_9	0.7261
k_{10}	-0.05721
k_{11}	-0.005238
k_{12}	1.370
k_{13}	-1.319

Table 3. Fitting formula constants for SIS haloes.

Name	Value for $f_{\text{DM}} < 0.55$	Value for $f_{\text{DM}} \geq 0.55$
k_1	2.546	2.546
k_2	0.6363	0.6363
k_3	0.1754	0.1754
k_4	1.097	1.097
k_5	3.779	3.779
k_6	-0.3725	-43.72
k_7	0.2549	38.30
k_8	-1.007	0
k_9	0.7579	0
k_{10}	-0.1034	47.96
k_{11}	0.8789	-42.32
k_{12}	-2.0134	0
k_{13}	2.094	0

$$f_1(x) = k_1(x/k_2)^{k_3} 10^{-k_4(x/k_2)^{k_5}} \quad (30)$$

$$f_2(x) = k_6 + k_7(x/0.5) + k_8(x/0.5)^2 + k_9(x/0.5)^3 \quad (31)$$

$$f_3(x) = k_{10} + k_{11}(x/0.5) + k_{12}(x/0.5)^2 + k_{13}(x/0.5)^3 \quad (32)$$

where n is the Sérsic index, f_{DM} is the 3D fraction of dark matter to total matter within the projected baryonic half-light radius, and the constants k_1 through k_{13} are given in Table 2. This approximation is accurate to 8% for Sérsic indices between 1 and 8 and dark matter fractions between 5% and 70%. This formula gives the values for $r_{\text{NFW}}/r_{\text{eff}} = 20$ and is subject to modification described above.

Figure 9 gives $r_{\text{eq}}/r_{\text{eff}}$ and $M_{\text{eq}}/M_{\text{bar}}$ for different central dark matter fractions under the assumption that the total density profile is that of a singular isothermal sphere. For a fixed baryonic mass and effective radius, the dark matter fraction within one baryonic projected half-light radius is adjusted by changing the SIS parameter s .

In this case r_{eq} and M_{eq} may be approximated by the same set of equations as for the case of an NFW halo: equations 29 through 32. Constants for the equations are given in Table 3. This approximation is accurate to 5% for Sérsic indices between 1 and 8 and dark matter fractions between 0.05 and 0.7, except near the transition between the two sets of fitting formula constants at $f_{\text{DM}} = 0.55$, where the approximation is only good to 20%.

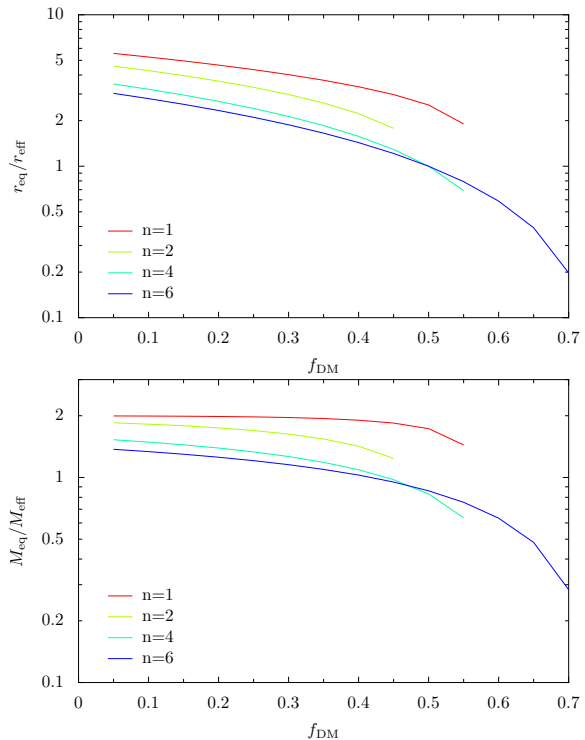


Figure 9. The relationship between our preferred dimensional scaling constants and directly observable quantities for a variety of mass models. The upper panel shows $r_{\text{eq}}/r_{\text{eff}}$ while the lower panel shows $M_{\text{eq}}/M_{\text{eff}}$, both as a function of the 3D dark matter fraction within the projected baryonic half-light radius. The parameter n is defined in equation 26 and gives the shape of the baryonic density profile. The dark matter fraction within one baryonic effective radius changes as a result of changes to the SIS density parameter s for a fixed baryonic model. The dominant consideration is the dark matter fraction, while the shape of the baryonic mass profile has a smaller effect.

6 CONCLUSIONS

We have considered the exact meaning of the concept of homology in the context of multi-component galaxies. A particularly useful formulation of the concept is termed *scaling-homology*. Using this definition, homology means that all galaxies are the same when scaled using the correct choice of length, mass, and time units, where the units are allowed to change from galaxy to galaxy. The three dimensional constants serve to fully specify a galaxy once the ‘master’ distribution function that describes all galaxies is known.

We used a set of hydrodynamical binary galaxy merger simulations spanning a range of masses, mass ratios, orbits, gas fractions, and supernova feedback prescriptions (but no AGN feedback) to determine the definition of dimensional scaling constants that served to make the remnants as close as possible to homologous. We found that the best definition of length, mass, and time units are r_{eq} , the radius within which dark and baryonic masses are equal, the mass within r_{eq} , and the dynamical time measured at r_{eq} . This is in contrast to the usual observationally motivated definitions of dimensional scaling constants: the baryonic half-light radius, the baryonic mass, and the central aperture velocity dispersion.

Simulated gas-rich binary galaxy merger remnants show

remarkably regular structure when the correct scale constants are used to plot dimensionless density and kinetic energy profiles. The stellar anisotropy is essentially the sole source of the variation in the kinematic structure of these simulated merger remnants. Dark halo concentration and progenitor gas fraction contribute to a systematic difference between the *Sbc* and *G* series simulations, but within each set of simulations the structure is remarkably consistent.

We emphasize that it is not *incorrect* to phrase questions about homology in terms of r_{eff} . Previous theoretical and observational studies that have done so have correctly asked and answered well-posed questions about galaxy scaling relations. However, we find that it is more informative to phrase questions about homology in terms of r_{eq} rather than r_{eff} , at least for our set of numerical simulations. Using r_{eff} , we would have concluded that our merger remnants are not homologous owing to a systematic change in the dark matter fraction within r_{eff} . However, if we instead scale by r_{eq} , we find that the merger remnants appear significantly more uniform. They are not perfectly homologous, but they are closer to homology than we would conclude based on r_{eff} . We are eager to learn whether the same holds true for numerical simulations by other groups and whether it holds true for actual galaxies.

In order to facilitate the use of these scaling constants to analyse actual galaxies, we calculated the ratios $r_{\text{eq}}/r_{\text{eff}}$ and $M_{\text{eq}}/M_{\text{bar}}$ for a set of observationally plausible two-component galaxy models and provided fitting formulas for the results.

The fact that r_{eq} plays such a prominent role in these scaling constants immediately recalls the disc-halo conspiracy arising from the study of spiral galaxy rotation curves (Bahcall & Casertano 1985; Burstein & Rubin 1985; Kent 1987). Blumenthal et al. (1986) argued that such a conspiracy will arise naturally if the dissipational collapse of baryons is limited by their initial angular momentum and if the baryon fraction is roughly equal to the spin parameter $\lambda = JE^{1/2}G^{-1}M^{-5/2}$. The result presented here appears to be another manifestation of this phenomenon. If the baryons have very little angular momentum, they will contract to the point where they are completely self-gravitating and the dark matter does not play a role in the dynamics, in which case r_{eff} and not r_{eq} is the important radius. On the other hand, if the baryons have too much angular momentum, they will not contract enough and the more massive dark matter halo will dominate the dynamics while the baryons function more as a tracer population. Simulated galaxy merger remnants are nearly homologous when r_{eq} rather than r_{eff} is used as the dimensional scaling constant, indicating that galaxies are in a ‘Goldilocks’ state where both baryons and dark matter play important dynamical roles. This is likely because of the initial balance between the baryon fraction and the spin parameter of dark matter haloes.

ACKNOWLEDGMENTS

We thank Michele Cappellari for useful discussions. GSN acknowledges the support of the Princeton University Council on Science and Technology. PJ acknowledges support by a grant from the W.M. Keck Foundation and by program HST-AR-11758, provided by NASA through a grant from

the Space Telescopes Research Institute, which is operated by the Association of Universities for Research in Astronomy, Incorporated, under NASA contract NAS5-26555.

This paper has been typeset from a $\text{T}_{\text{E}}\text{X}/\text{L}^{\text{A}}\text{T}_{\text{E}}\text{X}$ file prepared by the author.

REFERENCES

- Auger M. W., Treu T., Bolton A. S., Gavazzi R., Koopmans L. V. E., Marshall P. J., Moustakas L. A., Burles S., 2010, *ApJ*, 724, 511
- Bacon R., Copin Y., Monnet G., Miller B. W., Allington-Smith J. R., Bureau M., Carollo C. M., Davies R. L., Emsellem E., Kuntschner H., Peletier R. F., Verolme E. K., de Zeeuw P. T., 2001, *MNRAS*, 326, 23
- Baes M., Gentile G., 2010, *ArXiv e-prints*
- Bahcall J. N., Casertano S., 1985, *ApJ*, 293, L7
- Barnabè M., Czoske O., Koopmans L. V. E., Treu T., Bolton A. S., 2011, *MNRAS*, 415, 2215
- Bell E. F., McIntosh D. H., Katz N., Weinberg M. D., 2003, *ApJS*, 149, 289
- Burstein D., Faber S. M., 1992, *ApJ*, 399, 462
- Binney J., Tremaine S., 1987, *Galactic dynamics*. Princeton, NJ, Princeton University Press, 1987, 747 p.
- Blanton M. R., Roweis S., 2007, *AJ*, 133, 734
- Blumenthal G. R., Faber S. M., Flores R., Primack J. R., 1986, *ApJ*, 301, 27
- Bolton A. S., Treu T., Koopmans L. V. E., Gavazzi R., Moustakas L. A., Burles S., Schlegel D. J., Wayth R., 2008, *ApJ*, 684, 248
- Boylan-Kolchin M., Ma C.-P., Quataert E., 2005, *MNRAS*, 362, 184
- Bruzual G., Charlot S., 2003, *MNRAS*, 344, 1000
- Bullock J. S., Kolatt T. S., Sigad Y., Somerville R. S., Kravtsov A. V., Klypin A. A., Primack J. R., Dekel A., 2001, *MNRAS*, 321, 559
- Burstein D., Rubin V. C., 1985, *ApJ*, 297, 423
- Cappellari M., Bacon R., Bureau M., Damen M. C., Davies R. L., de Zeeuw P. T., Emsellem E., Falcón-Barroso J., Krajnović D., Kuntschner H., McDermid R. M., Peletier R. F., Sarzi M., van den Bosch R. C. E., van de Ven G., 2006, *MNRAS*, 366, 1126
- Cappellari M., et al., 2012, *ArXiv e-prints*
- Cox T. J., Jonsson P., Primack J. R., Somerville R. S., 2006, *MNRAS*, 373, 1013
- Czoske O., Barnabè M., Koopmans L. V. E., Treu T., Bolton A. S., 2008, *MNRAS*, 384, 987
- Dekel A., Cox T. J., 2006, *MNRAS*, 370, 1445
- Dekel A., Stoehr F., Mamon G. A., Cox T. J., Novak G. S., Primack J. R., 2005, *Nature*, 437, 707
- Diemand J., Kuhlen M., Madau P., Zemp M., Moore B., Potter D., Stadel J., 2008, *Nature*, 454, 735
- Djorgovski S., Davis M., 1987, *ApJ*, 313, 59
- Dressler A., Lynden-Bell D., Burstein D., Davies R. L., Faber S. M., Terlevich R., Wegner G., 1987, *ApJ*, 313, 42
- Gallazzi A., Charlot S., Brinchmann J., White S. D. M., Tremonti C. A., 2005, *MNRAS*, 362, 41
- Gavazzi R., Treu T., Koopmans L. V. E., Bolton A. S., Moustakas L. A., Burles S., Marshall P. J., 2008, *ApJ*, 677, 1046

- Gavazzi R., Treu T., Rhodes J. D., Koopmans L. V. E., Bolton A. S., Burles S., Massey R. J., Moustakas L. A., 2007, *ApJ*, 667, 176
- Gerhard O., Kronawitter A., Saglia R. P., Bender R., 2001, *AJ*, 121, 1936
- González-García A. C., van Albada T. S., 2003, *MNRAS*, 342, L36
- Graves G. J., Faber S. M., 2010, *ApJ*, 717, 803
- Grillo C., 2010, *ApJ*, 722, 779
- Grillo C., Gobat R., 2010, *MNRAS*, 402, L67
- Hopkins P. F., Cox T. J., Hernquist L., 2008, *ApJ*, 689, 17
- Humphrey P. J., Buote D. A., 2010, *MNRAS*, 403, 2143
- Jonsson P., 2006, *MNRAS*, 372, 2
- Jonsson P., Groves B. A., Cox T. J., 2010, *MNRAS*, 403, 17
- Kauffmann G., Heckman T. M., Tremonti C., Brinchmann J., Charlot S., White S. D. M., Ridgway S. E., Brinkmann J., Fukugita M., Hall P. B., Ivezić Ž., Richards G. T., Schneider D. P., 2003, *MNRAS*, 346, 1055
- Kent S. M., 1987, *AJ*, 93, 816
- Koopmans L. V. E., Bolton A., Treu T., Czoske O., Auger M. W., Barnabè M., Vegetti S., Gavazzi R., Moustakas L. A., Burles S., 2009, *ApJ*, 703, L51
- Lima Neto G. B., Gerbal D., Márquez I., 1999, *MNRAS*, 309, 481
- Mamon G. A., Lokas E. L., 2005, *MNRAS*, 362, 95
- Mazure A., Capelato H. V., 2002, *A&A*, 383, 384
- Navarro J. F., Frenk C. S., White S. D. M., 1996, *ApJ*, 462, 563
- Prugniel P., Simien F., 1997, *A&A*, 321, 111
- Robertson B., Cox T. J., Hernquist L., Franx M., Hopkins P. F., Martini P., Springel V., 2006, *ApJ*, 641, 21
- Schwarzschild M., 1979, *ApJ*, 232, 236
- Sersic ed. 1968, *Atlas de galaxias australes*. Cordoba, Argentina: Observatorio Astronomico, 1968
- Taylor E. N., Franx M., Brinchmann J., van der Wel A., van Dokkum P. G., 2010, *ApJ*, 722, 1
- Thomas J., Saglia R. P., Bender R., Thomas D., Gebhardt K., Magorrian J., Corsini E. M., Wegner G., 2007, *MNRAS*, 382, 657
- Thomas J., Saglia R. P., Bender R., Thomas D., Gebhardt K., Magorrian J., Corsini E. M., Wegner G., 2009, *ApJ*, 691, 770
- Trujillo I., Asensio Ramos A., Rubiño-Martín J. A., Graham A. W., Aguerri J. A. L., Cepa J., Gutiérrez C. M., 2002, *MNRAS*, 333, 510
- van Dokkum P. G., Conroy C., 2011, *ApJ*, 735, L13+
- York D. G., et al., 2000, *AJ*, 120, 1579